








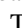

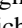

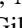





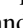





SCEXAO/CHARIS Direct Imaging Discovery of a 20 au Separation, Low-mass Ratio Brown Dwarf Companion to an Accelerating Sun-like Star*

Thayne Currie^{1,2,3} , Timothy D. Brandt⁴ , Masayuki Kuzuhara^{5,6} , Jeffrey Chilcote⁷, Olivier Guyon^{1,5,8,9} , Christian Marois^{10,11} , Tyler D. Groff¹², Julien Lozi¹ , Sebastien Vievard¹, Ananya Sahoo¹ , Vincent Deo¹, Nemanja Jovanovic¹³ , Frantz Martinache¹⁴ , Kevin Wagner^{8,25} , Trent Dupuy^{15,16} , Matthew Wahl¹, Michael Letawsky¹, Yiting Li⁴, Yunlin Zeng¹⁷, G. Mirek Brandt⁴ , Daniel Michalik¹⁸ , Carol Grady³, Markus Janson¹⁹ , Gillian R. Knapp²⁰ , Jungmi Kwon²¹ , Kellen Lawson²² , Michael W. McElwain¹² , Taichi Uyama²³ , John Wisniewski²² , and Motohide Tamura^{5,6,24} 

¹ Subaru Telescope, National Astronomical Observatory of Japan, 650 North A'ohōkū Place, Hilo, HI 96720, USA; currie@naoj.org

² NASA-Ames Research Center, Moffett Boulevard, Moffett Field, CA, USA

³ Eureka Scientific, 2452 Delmer Street, Suite 100, Oakland, CA, USA

⁴ Department of Physics, University of California, Santa Barbara, Santa Barbara, CA, USA

⁵ Astrobiology Center of NINS, 2-21-1, Osawa, Mitaka, Tokyo 181-8588, Japan

⁶ National Astronomical Observatory of Japan, 2-21-2, Osawa, Mitaka, Tokyo 181-8588, Japan

⁷ Department of Physics, University of Notre Dame, South Bend, IN, USA

⁸ Steward Observatory, The University of Arizona, Tucson, AZ 85721, USA

⁹ College of Optical Sciences, The University of Arizona, Tucson, AZ 85721, USA

¹⁰ National Research Council of Canada Herzberg, 5071 West Saanich Road, Victoria, BC V9E 2E7, Canada

¹¹ Department of Physics and Astronomy, University of Victoria, 3800 Finnerty Road, Victoria, BC V8P 5C2, Canada

¹² NASA-Goddard Space Flight Center, Greenbelt, MD, USA

¹³ Department of Astronomy, California Institute of Technology, 1200 E. California Boulevard, Pasadena, CA 91125, USA

¹⁴ Université Côte d'Azur, Observatoire de la Côte d'Azur, CNRS, Laboratoire Lagrange, France

¹⁵ Institute for Astronomy, University of Edinburgh, Blackford Hill, Edinburgh EH9 3HJ, UK

¹⁶ Centre for Exoplanet Science, University of Edinburgh, Edinburgh, UK

¹⁷ School of Physics, Georgia Institute of Technology, 837 State Street, Atlanta, GA, USA

¹⁸ European Space Agency (ESA/ESTEC): Noordwijk, South Holland, Netherlands

¹⁹ Department of Astronomy, Stockholm University, AlbaNova University Center, SE-10691 Stockholm, Sweden

²⁰ Department of Astrophysical Sciences, Princeton University, Princeton, NJ, USA

²¹ ISAS/JAXA, 3-1-1 Yoshinodai, Chuo-ku, Sagami-hara, Kanagawa 252-5210, Japan

²² Homer L. Dodge Department of Physics, University of Oklahoma, Norman, OK 73071, USA

²³ Infrared Processing and Analysis Center, California Institute of Technology, Pasadena, CA 91125, USA

²⁴ Department of Astronomy, Graduate School of Science, The University of Tokyo, 7-3-1, Hongo, Bunkyo-ku, Tokyo 113-0033, Japan

Received 2020 September 19; revised 2020 October 21; accepted 2020 October 30; published 2020 November 30

Abstract

We present the direct imaging discovery of a substellar companion to the nearby Sun-like star, HD 33632 Aa, at a projected separation of ~ 20 au, obtained with SCEXAO/CHARIS integral field spectroscopy complemented by Keck/NIRC2 thermal infrared imaging. The companion, HD 33632 Ab, induces a 10.5σ astrometric acceleration on the star as detected with the Gaia and Hipparcos satellites. SCEXAO/CHARIS *JHK* (1.1–2.4 μm) spectra and Keck/NIRC2 L_p (3.78 μm) photometry are best matched by a field L/T transition object: an older, higher-gravity, and less dusty counterpart to HR 8799 cde. Combining our astrometry with Gaia/Hipparcos data and archival Lick Observatory radial velocities, we measure a dynamical mass of $46.4 \pm 8 M_J$ and an eccentricity of $e < 0.46$ at 95% confidence. HD 33632 Ab's mass and mass ratio ($4.0\% \pm 0.7\%$) are comparable to the low-mass brown dwarf GJ 758 B and intermediate between the more massive brown dwarf HD 19467 B and the (near-)planet-mass companions to HR 2562 and GJ 504. Using Gaia to select for direct imaging observations with the newest extreme adaptive optics systems can reveal substellar or even planet-mass companions on solar system-like scales at an increased frequency compared to blind surveys.

Unified Astronomy Thesaurus concepts: Exoplanets (498); Brown dwarfs (185); Astronomical instrumentation (799); Astronomical optics (88); Direct imaging (387); Coronagraphic imaging (313); Exoplanet detection methods (489); Astronomical techniques (1684)

1. Introduction

Facility and now extreme adaptive optics systems have provided the first direct detections of exoplanets around nearby, young stars (Marois et al. 2008, 2010; Kuzuhara et al. 2013; Currie et al. 2014b, 2015; Macintosh et al. 2015; Keppler et al. 2018).

Blind direct imaging surveys have provided the first constraints on the frequency of Jovian planets and low-mass brown dwarfs at orbital distances of 10–500 au (Brandt et al. 2014; Nielsen et al. 2019).

Unfortunately, the low yield of blind direct imaging surveys shows that exoplanets detectable with current instruments are rare (e.g., Nielsen et al. 2019), especially around solar- and subsolar-mass stars. The few companions found by these surveys typically exceed five Jovian masses and orbit well beyond separations where the Jovian planet frequency peaks

* Based in part on data collected at Subaru Telescope, which is operated by the National Astronomical Observatory of Japan.

²⁵ NASA Hubble/Sagan Fellow, NASA Nexus for Exoplanet System Science, Earths in Other Solar Systems Team.

Table 1
HD 33632 Observing Log

UT Date	Instrument	Seeing ^a (")	Filter	λ (μm) ^b	t_{exp}	N_{exp}	ΔPA ($^\circ$)	Reduction Strategy	S/N ^c (HD 33632 Ab)
20181018	SCEXAO/CHARIS ^b	0.5	<i>JHK</i>	1.16–2.37	45.7	14	3.0	SDI	22
20181101	Keck/NIRC2	0.7	L_p	3.78	50	26	13.9	ADI	11
20200831	SCEXAO/CHARIS ^b	0.6	<i>JHK</i>	1.16–2.37	31	86	17.8	ADI, ADI+SDI	41
20200901	SCEXAO/CHARIS ^{b,d}	0.5–1.0	<i>JHK</i>	1.16–2.37	45.7	26	20.8	ADI, ADI+SDI	27

Notes.

^a From the Canada–France–Hawaii Telescope seeing monitor.

^b For CHARIS data, this column refers to the wavelength range. For NIRC2 imaging data, it refers to the central wavelength.

^c The S/N of HD 33632 Ab in the wavelength-collapsed image reduced using “conservative” ADI/A-LOCI algorithm settings or SDI/A-LOCI for the case of 2018 October SCEXAO/CHARIS data.

^d Twenty-six frames (~ 20 minutes) of the 2020 August 31 data were also obtained with the star dithered by $1''.1$ to the north and east.

(Fernandes et al. 2019). Improving blind survey yields will only be possible with substantial contrast gains at small separations and/or sensitivity gains at wider separations (Crepp & Johnson 2011). Limited sample sizes and sparse coverage of ages, temperatures, and surface gravities impede our understanding of the atmospheric evolution of gas giant planets.

Targeted searches focused on stars showing evidence of gravitational pulls from massive planets could improve survey yields. While radial-velocity data have been used for sample selection with some success for finding (sub)stellar companions (Crepp et al. 2014), astrometry can also select direct imaging targets, even around stars whose activity and spectral type preclude precise radial-velocity measurements. The Hipparcos-Gaia Catalog of Accelerations (HGCA; Brandt 2018) provides absolute astrometry for 115,000 nearby stars, including those with clear dynamical evidence for unseen massive companions. HGCA-derived accelerations can provide dynamical masses of imaged exoplanets and low-mass brown dwarfs independent of luminosity evolution models and irrespective of stellar age uncertainties (Brandt et al. 2019; Dupuy et al. 2019).

In this Letter, we report the direct imaging discovery of a low-mass substellar companion 20 au from the nearby Sun-like star HD 33632 Aa using the Subaru Coronagraphic Extreme Adaptive Optics Project (SCEXAO; Jovanovic et al. 2015b) coupled to the CHARIS integral field spectrograph (Groff et al. 2016) and using the NIRC2 camera on Keck. The HGCA identifies an astrometric acceleration for the primary induced by HD 33632 Ab, providing a dynamical mass of $46 \pm 8 M_J$ for the companion. CHARIS spectra and NIRC2 photometry reveal HD 33632 Ab to be a higher-gravity, higher-mass counterpart to young L/T transition planet-mass objects such as HR 8799 cde with a low eccentricity more typical of directly imaged planets than brown dwarfs.

2. Systems Properties, Observations, and Data

The HD 33632 primary is a 26.56 pc distant F8V 1.1 M_\odot main-sequence star (Takeda et al. 2007; Gaia Collaboration et al. 2018). The star has an M-star companion, 2MASS J05131845+3720463, at $\rho \sim 34''$ (900 au; Scholz 2016) with the same parallax as HD 33632 Aa and a proper motion difference of $\sim 3 \text{ mas yr}^{-1}$ (Brandt 2018; Gaia Collaboration et al. 2018).²⁶

²⁶ The Washington Double Star Catalog lists the system as WDS J05133+3720A and WDS J05133+3720B; a third interloping star is mislabeled as WDS J05133+3720C. To avoid confusion, we describe the primary as HD 33632 Aa and the companion as HD 33632 Ab.

Age estimates for the HD 33632 primary drawn from CaHK measurements ($\log(R'_{\text{HK}}) = -4.76$ to -4.93) encompass ~ 1.2 – 4.5 Gyr (e.g., Takeda et al. 2007; Pace 2013). The Mamajek & Hillenbrand (2008) activity–rotation–age relation and gyrochronology as implemented in Brandt et al. (2014) favor the low end of this range (~ 1 – 2.5 Gyr). HD 33632 Aa’s fractional X-ray luminosity ($\log(L_X/L_{\text{bol}} = -5.2)$) overlaps with those for 800 Myr old Hyades stars (Brandt & Huang 2015; Freund et al. 2020). Li abundances are consistent with the Hyades but marginally consistent with 4 Gyr old M67 (Ramírez et al. 2012; Castro et al. 2016). Ages estimated using neutron-capture elements abundances individually (e.g., [Zr/Fe]) or in aggregate (e.g., the average abundances of “heavy” elements Ce, Ba, and La; [Y/Mg]) cluster around 1.5–2.5 Gyr (Spina et al. 2018). Given activity, gyrochronology, and neutron-capture abundance-derived estimates, we adopt a broad age range of $1.5_{-0.7}^{+3.0}$ Gyr with a preference for 1.0–2.5 Gyr.

HGCA reveals the HD 33632 primary to have a statistically significant acceleration ($\chi^2 \approx 116$) for a model of constant proper motion, equivalent to 10.5σ with 2 degrees of freedom: evidence for the dynamical pull of a companion. The acceleration is almost 1000 times larger than that expected from the M-dwarf companion. The Lick radial-velocity survey monitored HD 33632 Aa for 11 years (1998 January 18 to 2009 February 1) without finding evidence of a planet or brown dwarf (Fischer et al. 2014): the companion must be widely separated. Following estimates in Brandt et al. (2019), its minimum mass at angles accessible by SCEXAO/CHARIS ($\rho \sim 0''.1$ – $1''.05$) ranges from a few Jovian masses to over $50 M_J$.

Table 1 summarizes our observations with SCEXAO/CHARIS and Keck/NIRC2 in 2018 and 2020. The seeing ranged between $\theta_v = 0''.4$ and $1''.0$; conditions were photometric each night. SCEXAO achieved a high-fidelity AO correction; we utilized the CHARIS integral field spectrograph (Groff et al. 2016) in low spectral resolution (broadband) mode covering the *JHK* passbands simultaneously (1.16–2.37 μm at $\mathcal{R} \sim 18$). NIRC2 data were taken in the L_p broadband filter ($\lambda_o = 3.78 \mu\text{m}$) using Keck’s facility AO system.

All CHARIS data utilized satellite spots for precise astrometric and spectrophotometric calibration (Jovanovic et al. 2015a). The CHARIS data were taken with a Lyot coronagraph ($0''.139$ radius occulting mask); the NIRC2 data were taken behind a Lyot coronagraph with a $0''.2$ radius occulting mask. All observations were conducted in pupil-tracking mode, enabling angular differential imaging (ADI; Marois et al. 2006); the CHARIS data also enable spectral differential imaging (SDI; Marois et al. 2000).

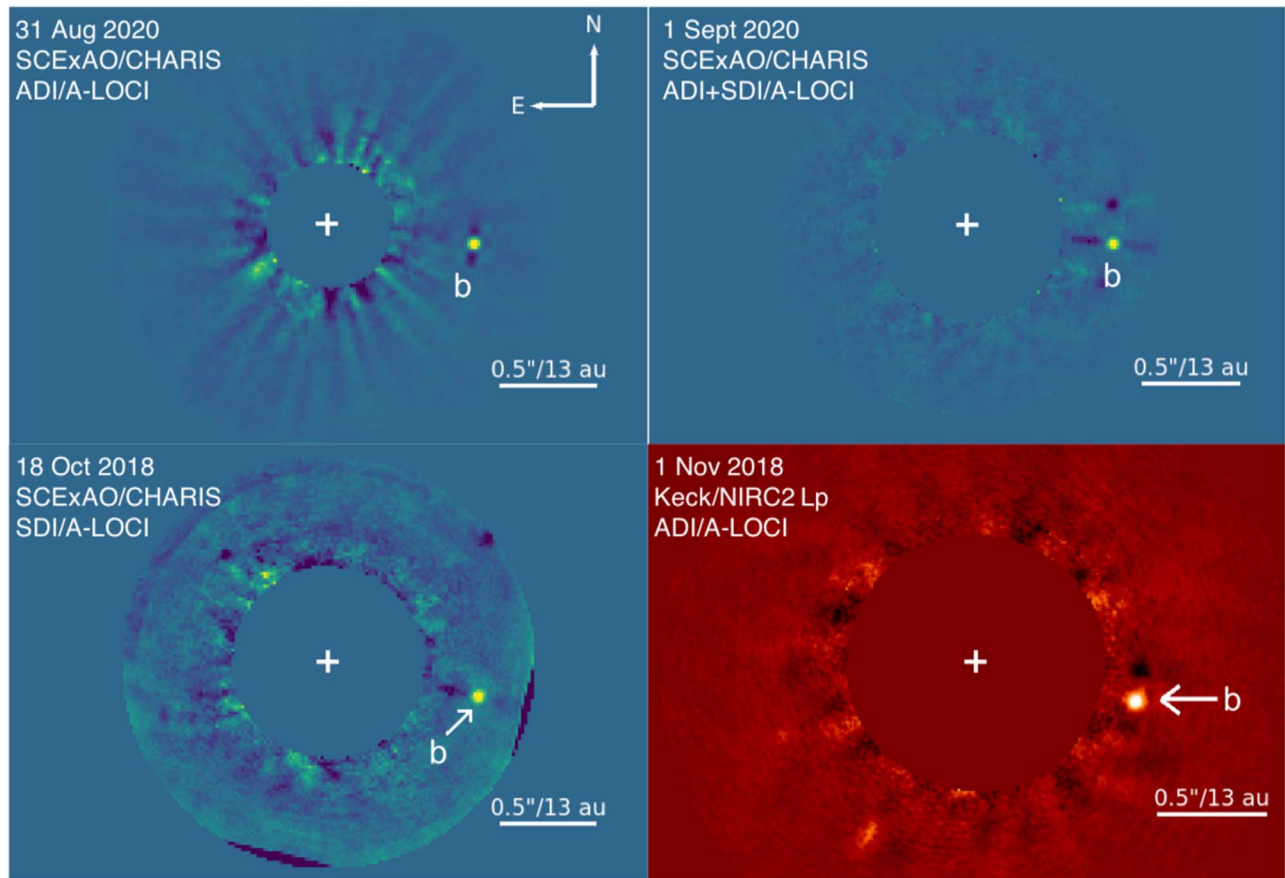


Figure 1. HD 33632 Ab detections in 2020 (top panels) and 2018 (bottom panels) reduced using A-LOCI with different combinations of ADI, SDI, and ADI+SDI. Our adopted rotation gap/radial scaling criteria preclude access to masked regions.

We extracted CHARIS data cubes using the standard CHARIS pipeline (Brandt et al. 2017) and performed basic reduction steps including sky subtraction, image registration, and spectrophotometric calibration as in Currie et al. (2018). For spectrophotometric calibration, we adopted a Kurucz stellar atmosphere model appropriate for an F8V star. We reduced the NIRC2 data using the ADI-based pipeline from Currie et al. (2011).

For all data, we used A-LOCI for point-spread function (PSF) subtraction (Currie et al. 2018). Due to a lack of field rotation, we subtracted the PSF for the 2018 CHARIS data in SDI mode only. The 2020 CHARIS data enabled PSF subtraction with ADI, SDI, and ADI+SDI (i.e., performing SDI on the A-LOCI PSF subtraction residuals produced from ADI). In all cases, we used a large rotation gap/radial scaling criterion of $\delta > 1 \lambda/D$ to limit self-subtraction. For the CHARIS SDI reduction (component), we employed a pixel mask over the subtraction zone (Marois et al. 2010; Currie et al. 2015) to significantly reduce biasing of a companion spectrum.

Figure 1 shows the detection of a faint point source, hereafter HD 33632 Ab, $\rho \approx 0''.75$ west from the primary in each epoch. The detection’s signal-to-noise ratios (S/Ns) in conservative ADI/A-LOCI or SDI/A-LOCI reductions range between 11–22 in the 2018 discovery epoch to 41 for the 2020 August 31 CHARIS broadband follow-up data. CHARIS data do not identify any other companion within $\rho \sim 1''.05$. In addition to resolving HD 33632 Ab, NIRC2 data identify a wider separation object at $[E, N]'' = [-1''.22, -1''.85]$ and $L_p \sim 16.3$ (not shown). However, 2020 CHARIS data reveal this object to be

a background star based on its astrometry and its near-infrared brightness.

3. Analysis

3.1. Infrared Colors, Spectrum, and Atmosphere of HD 33632 Ab

To derive throughput-corrected spectrophotometry, we forward-modeled point sources at HD 33632 Ab’s locations using stored LOCI coefficients (Currie et al. 2018). We focus on ADI-only reductions due to the more straightforward applicability of ADI-reduced data to forward modeling (Pueyo 2016). We adopt our highest-quality data set (2020 August 31) for our analyses. Our results agree with those from other data sets and with SDI reductions.

We extract spectra from the best-fit centroid position of the wavelength-collapsed image. Throughputs typically exceed 75%; because we use ADI only, they are independent of HD 33632 Ab’s spectrum. HD 33632 Ab’s broadband photometry in standard Maunakea Observatory filters is $J = 16.91 \pm 0.11$, $H = 16.00 \pm 0.09$, $K_s = 15.37 \pm 0.09$, and $L_p = 13.67 \pm 0.15$ ($\Delta J, H, K_s = 11.52, 10.83, 10.21$). Photometry obtained at different epochs or with different reductions agrees with these results to within errors.

HD 33632 Ab lies at the transition from cloudy L dwarfs to (nearly) cloud-free T dwarfs (Burrows et al. 2006). Figure 2 places it on an infrared color–magnitude diagram. The companion’s $J/J-K_s$ position is consistent with field L/T objects, while its $L_p/H-L_p$ position agrees with both field

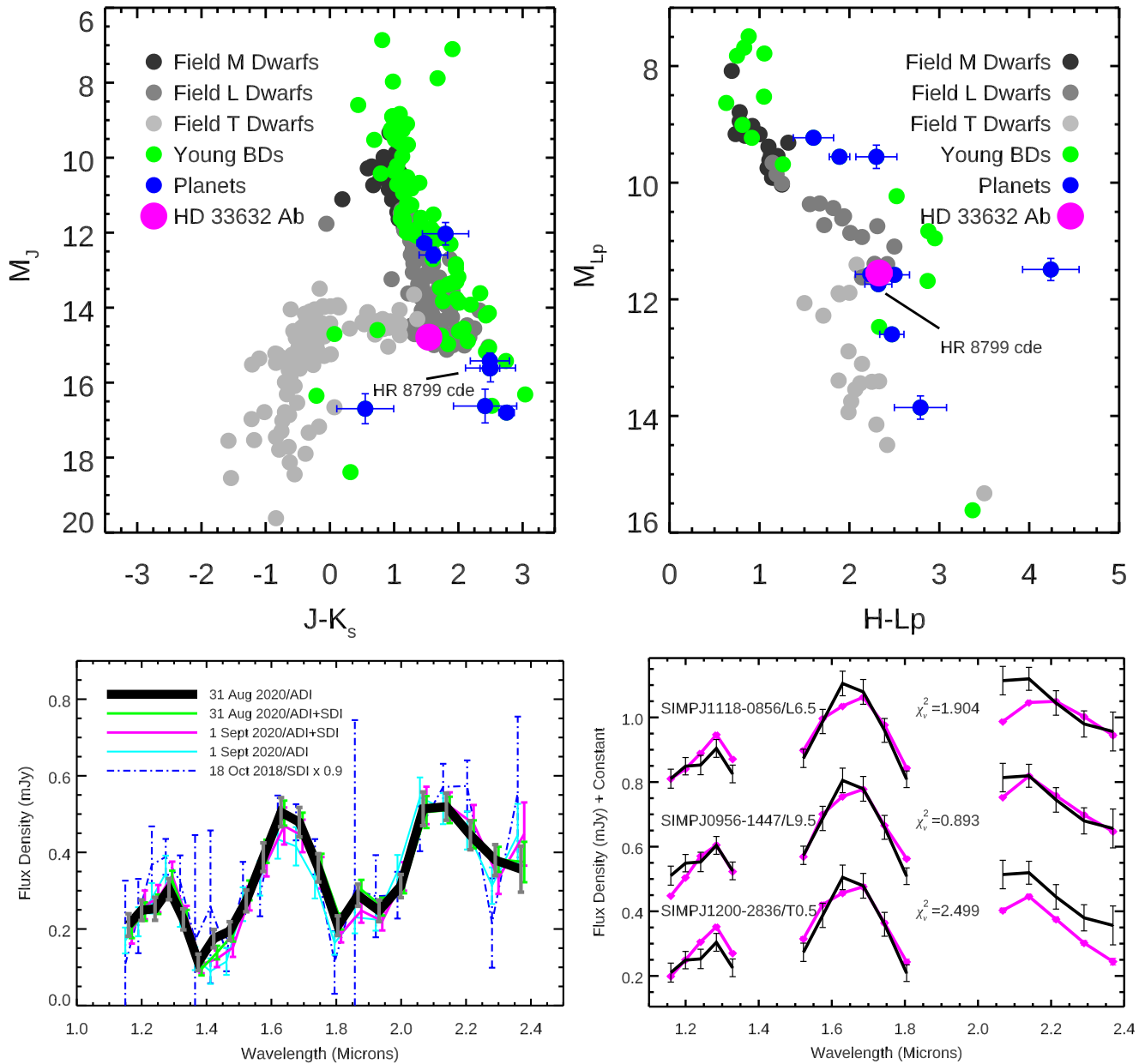


Figure 2. (Top) J/K_s and $L_p/H-L_p$ color–magnitude diagram comparing field/young low-mass MLT-type (sub)stellar objects, directly imaged exoplanets, and HD 33632 Ab. Data draw from Dupuy & Liu (2012) with updated photometry for directly imaged planets: e.g., HR 8799 bcde (drawn from Currie et al. 2014a; Zurlo et al. 2016). (Bottom left) CHARIS spectrum extracted from 2020 August 31 data reduced with ADI/A-LOCI (thick black line, gray error bars) compared to spectra extracted on different nights or with different processing. (Bottom right) The CHARIS HD 33632 Ab spectrum (black) compared to field brown dwarf spectra (magenta) near the L/T transition from the Montreal Spectral Library (binned to CHARIS’s resolution).

objects and the low-gravity, cloudy exoplanets HR 8799 cde (Currie et al. 2011; Barman et al. 2015).

The CHARIS spectrum of HD 33632 Ab (Figure 2, bottom-left panel; Table 2) is highly peaked, characteristic of a substellar atmosphere shaped by water opacity. The 2018 CHARIS spectrum is significantly noisier and offset by $\sim 10\%$ compared to the 2020 epoch data. Otherwise, spectra extracted using different reduction techniques and taken on different epochs agree to within errors. The detection significance of HD 33632 Ab reaches $S/N = 20\text{--}30$ in some channels for the 2020 August 31/ADI-reduced spectrum. However, contributions from uncertainties in the absolute flux calibration (i.e., the satellite spot flux uncertainty) limit the spectrophotometric precision to about 10%.

We compared HD 33632 Ab’s CHARIS spectrum to objects in the Montreal Spectral Library²⁷ (e.g., Gagné et al. 2014), considering the impact of spatially and spectrally correlated noise (Greco & Brandt 2016). The spectral covariance at HD 33632 Ab’s angular separation in the 2020 August 31 ADI/A-LOCI reduced data is nearly zero for off-diagonal elements indicating largely uncorrelated noise.

The L9.5 field brown dwarfs SIMPJ0956-1447 and SIMPJ0150+3827 provide the best fit to HD 33632 Ab’s spectrum (Figure 2, bottom-right panel). While the Montreal library contains few objects later than L5, the χ^2 distribution for library objects exhibits a local minimum between L6.5 and

²⁷ <https://jgagneastro.com/the-montreal-spectral-library/>

Table 2
HD 33632 Ab Spectrum

Wavelength (μm)	F_ν (mJy)	σF_ν (mJy)	S/N
1.160	0.210	0.029	8.9
1.200	0.249	0.027	12.6
1.241	0.253	0.030	10.7
1.284	0.304	0.028	13.9
1.329	0.225	0.027	10.7
1.375	0.113	0.022	5.5
1.422	0.175	0.024	8.1
1.471	0.195	0.024	9.3
1.522	0.273	0.028	13.0
1.575	0.387	0.037	14.4
1.630	0.505	0.038	21.3
1.686	0.479	0.038	20.8
1.744	0.360	0.037	16.1
1.805	0.209	0.026	10.2
1.867	0.288	0.029	13.0
1.932	0.247	0.028	10.9
1.999	0.312	0.030	14.2
2.068	0.514	0.044	28.0
2.139	0.519	0.035	30.1
2.213	0.445	0.038	22.7
2.290	0.380	0.040	12.7
2.369	0.356	0.060	6.5

Note. Throughput-corrected HD 33632 Ab spectrum extracted from 2020 August 31 data, reduced using ADI/A-LOCI.

T0.5. Thus, conservatively we assign HD 33632 Ab a spectral type of L9.5 $_{-3.0}^{+1.0}$. Adopting the mapping between spectral type and temperature from Stephens et al. (2009), the object’s effective temperature is 1300 $_{-100}^{+100}$ K: slightly higher than that derived for the inner three HR 8799 planets (Currie et al. 2011; Barman et al. 2015). Adopting the polynomial fit from Golimowski et al. (2004) and a distance of 26.56 pc, HD 33632 Ab’s luminosity is $\log_{10}(L/L_{\odot}) = -4.62_{-0.08}^{+0.04}$.

3.2. Astrometry and Common Proper Motion

As our forward modeling revealed negligible astrometric bias and different reductions yielded consistent astrometry, we used Gaussian centroiding to determine the position of HD 33632 Ab. HD 33632 Ab is located at [E, N] $'' = [-0.''761, -0.''176] \pm [0.''005, 0.''004]$ and $[-0.''753, -0.''178] \pm [0.''005, 0.''005]$ in the 2018 CHARIS and NIRC2 data, respectively: the same within errors. Our errors consider the centroiding precision and uncertainties in the pixel scale and true north.²⁸

In the 2020 CHARIS data, HD 33632 Ab’s position is [E, N] $'' = [-0.''740, -0.''095] \pm [0.''005, 0.''003]$. Between 2018 October and 2020 August, a background star would be offset to the northeast by $\sim[0.''24, 0.''18]$, inconsistent with HD 33632 Ab’s observed displacement of $[0.''021, 0.''081]$.

3.3. Orbit and Dynamical Mass

We use the open-source code `orvara` (Brandt et al. 2020) to fit HD 33632 Ab’s mass and orbit using a combination of

²⁸ We reassessed the pixel scale and north position angle estimate for the 2020 data, following Currie et al. (2018) in using contemporaneous Keck/NIRC2 astrometry for HD 1160 B (Nielsen et al. 2012) taken on 2020 July 9. Adopting a north position angle of -2.2° and pixel scale of $0.''0162$ as in Currie et al. (2018), HD 1160 B’s positions with NIRC2 and CHARIS agree to within 4 mas, well within errors.

HGCA measurements, Lick Observatory radial-velocity data (Fischer et al. 2014), and relative astrometry from CHARIS and NIRC2. No other bound companion is detected with CHARIS, Lick data do not identify an inner companion, and the only other object seen with NIRC2 is a background star. Given its separation, the M-dwarf companion contributes $<1\%$ of the acceleration seen by HGCA. Therefore, we assume that HD 33632 Ab is solely responsible for the HGCA acceleration. The astrometric acceleration of $\sim 0.1 \text{ mas yr}^{-2}$ is more than 1000 times smaller than the apparent acceleration due to parallactic motion: it negligibly affects the Gaia parallax. We fit for a radial-velocity jitter, the six Keplerian orbital elements, and the masses of both components. We adopt a prior on HD 33632 Aa’s mass of $1.1 \pm 0.1 M_{\odot}$ and a log-uniform prior on the mass of HD 33632 Ab. We analytically marginalize out the nuisance parameters of barycenter proper motion, parallax, and radial-velocity zero-point.

Figure 3 shows our posterior distributions for selected orbital parameters, the primary mass (almost identical to our prior of $1.1 \pm 0.1 M_{\odot}$), and HD 33632 Ab’s mass. Table 3 lists all priors and posteriors from the fit. The companion has a best-fit semimajor axis of $21.2_{-4.5}^{+4.1}$ au with an orbit inclined by $i = 39.4_{-20}^{+8.0}$. The semimajor axis is double-peaked because our relative astrometry spans only a 2 yr baseline, while there is a 25 yr elapse between absolute astrometric measurements: Hipparcos mainly constrains HD 33632 Ab’s 1991 position. Continued orbital monitoring will remove the double peak, improving the companion’s mass measurement. HD 33632 Ab’s median posterior eccentricity is $e = 0.19$ but the distribution peaks at zero (i.e., a circular orbit): the 68% and 95% upper limits are 0.29 and 0.46, respectively.

HD 33632 Ab has a dynamical mass of $46.4_{-7.6}^{+8.1} M_J$ and a mass ratio of $q \sim 4.0\% \pm 0.7\%$. We may compare this to masses derived by matching its observed luminosity and age with substellar evolutionary models. For its full (preferred) age range of $1.5_{-0.7}^{+3.0}$ Gyr (1–2.5 Gyr), the Baraffe et al. (2003) and Burrows et al. (1997) luminosity evolution models imply masses of $48_{-9}^{+17} M_J$ (41–60 M_J) and $55_{-15}^{+18} M_J$ (45–65 M_J), respectively. These model-dependent masses agree well with the dynamical mass if we adopt our preferred age of 1–2.5 Gyr, but show moderate tension for ages $\gtrsim 2.5$ Gyr.

4. Discussion

Our SCExAO/CHARIS and complementary Keck/NIRC2 imaging identify a low-mass-ratio brown dwarf companion at $r_{\text{proj}} \sim 20$ au around the main-sequence Sun-like star, HD 33632 Aa. HD 33632 Ab’s infrared colors and spectrum are best matched by a field L/T transition object. Combining measurements from Hipparcos, Gaia, and precision radial-velocity with our CHARIS/NIRC2 relative astrometry yields a dynamical mass of $46.4_{-7.6}^{+8.1} M_J$. This is more precise than estimates from luminosity evolution models alone, given age uncertainties, and it will improve with continued astrometric monitoring and future Gaia data releases. Provided that the system age and companion mass are better constrained in future work, HD 33632 Ab adds to the still-small sample of objects enabling us to test substellar evolutionary models across masses and ages.

HD 33632 Ab lies at the field L/T transition tracking the dissipation of clouds/dust in substellar atmospheres. In $L_p/H-L_p$, its colors overlap with and its temperature is just slightly exceeds those of the young exoplanets HR 8799 cde.

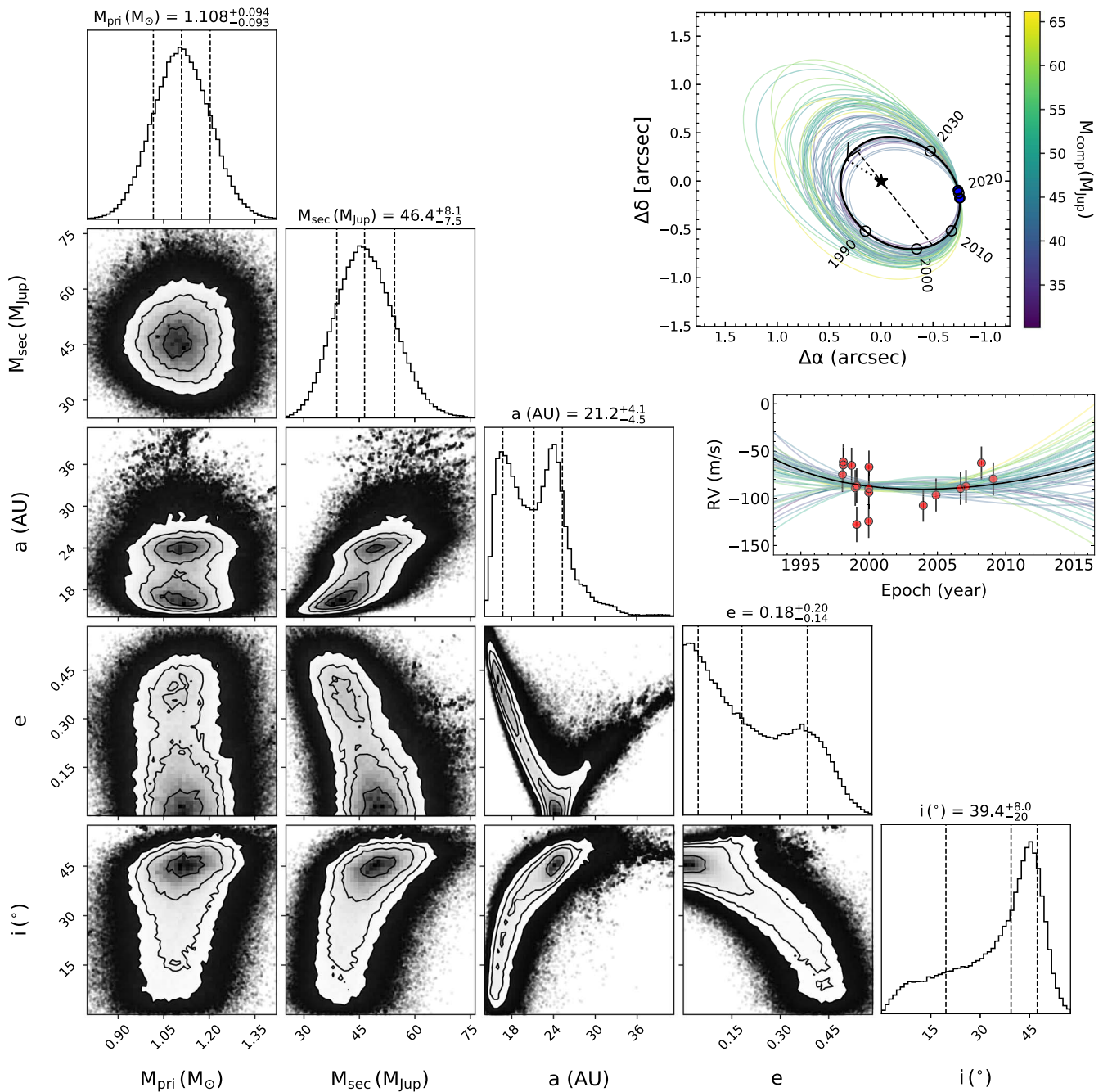


Figure 3. Corner plot showing posterior distributions of selected orbital parameters. The orbit fits used Hipparcos and Gaia absolute astrometry, Lick Observatory precision radial-velocity measurements for HD 33632 Aa, and relative astrometry of HD 33632 Ab. The posterior on HD 33632 Aa’s mass is dominated by our adopted prior of $1.1 \pm 0.1 M_{\odot}$. The insets display the best-fit orbit along with 100 random orbits drawn from our Markov Chain Monte Carlo in both relative astrometry and radial velocity, color-coded by HD 33632 Ab’s mass. Zero radial velocity corresponds to the system barycenter of the best-fit orbit (black curve); all radial-velocity data points and curves are shifted by the best-fit radial-velocity offsets to align with the black curve.

HD 33632 Ab represents an older, higher-mass, higher-gravity, and (likely) less cloudy/dusty counterpart to some of the first imaged exoplanets. Thermal infrared follow-up imaging and spectroscopy on the ground and with the James Webb Space Telescope could further clarify how its atmospheric chemistry compares with HR 8799 cde and other companions. Theoretical modeling incorporating these higher-resolution data will quantify constraints on HD 33632 Ab’s atmosphere.

HD 33632 Ab’s mass, mass ratio, and orbital separation are nearly identical to those of the older, colder brown dwarf companion GJ 758 B (Thalmann et al. 2009; Brandt et al. 2019),

which likewise orbits a Sun-like star. Its mass and mass ratio bracket those of other companions to mid-F to early-G stars orbiting at 20–50 au: e.g., the more massive, older T dwarf companion HD 19467 B (Crepp et al. 2014) and (near-)planet-mass companions HR 2562 b (Konopacky et al. 2016) and GJ 504 b (Kuzuhara et al. 2013) with comparable or younger ages.

HD 33632 Ab’s eccentricity posterior probability distribution has a 68% upper limit of 0.29. This is smaller than the eccentricities of most brown dwarfs studied in Bowler et al. (2020), who argue that systematically higher eccentricities of brown dwarf-mass companions relative to exoplanets point to a

Table 3
Markov Chain Monte Carlo Orbit Fitting Priors and Results

Parameter	16%/50%/84% Quantiles	95% Confidence Interval	Prior
Fitted Parameters			
RV jitter (m s^{-1})	$2.53^{+0.19}_{-0.18}$	(2.19, 2.91)	log-flat
$M_{\text{pri}} (M_{\odot})$	$1.108^{+0.094}_{-0.093}$	(0.93, 1.29)	Gaussian, 1.1 ± 0.1
$M_{\text{sec}} (M_{\text{Jup}})$	$46.4^{+8.1}_{-7.5}$	(32.5, 62.8)	$1/M_{\text{sec}}$ (log-flat)
Semimajor axis a (au)	$21.2^{+4.1}_{-4.5}$	(15.2, 30.9)	$1/a$ (log-flat)
$\sqrt{e} \sin \omega^{\text{a}}$	$0.05^{+0.21}_{-0.24}$	(-0.39, 0.47)	uniform
$\sqrt{e} \cos \omega^{\text{a}}$	$0.15^{+0.37}_{-0.52}$	(-0.62, 0.64)	uniform
Inclination ($^{\circ}$)	$39.4^{+8.0}_{-20}$	(6.0, 52.2)	$\sin i$ (geometric)
PA of the ascending node Ω ($^{\circ}$)	$38.2^{+7.2}_{-7.0}$	(21.3, 256)	uniform
Mean longitude at 2010.0 ($^{\circ}$)	21^{+14}_{-10}	(10.3, 286)	uniform
Parallax (mas)	37.647 ± 0.071	(37.52, 37.78)	Gaussian, 37.646 ± 0.064
Barycenter $\mu_{\alpha*}$ (mas yr^{-1})	-144.90 ± 0.13	(-145.15, -144.66)	uniform
Barycenter μ_{δ} (mas yr^{-1})	-135.21 ± 0.32	(-135.8, -134.55)	uniform
Radial-velocity zero-point (m s^{-1})	-129^{+31}_{-68}	(-246, 180)	uniform
Derived Parameters			
Period (yrs)	91 ± 27	(55, 160)	
Argument of periastron ω ($^{\circ}$) ^a	151^{+155}_{-131}	(4, 356)	
Eccentricity e	$0.18^{+0.20}_{-0.14}$	<0.46	
Semimajor axis (mas)	800^{+150}_{-170}	(570, 1160)	
Periastron time T_0 (JD)	2440900^{+4500}_{-13100}	(2404000, 2453500)	
Mass ratio	$0.0402^{+0.0078}_{-0.0073}$	(0.0267, 0.0563)	

Note.

^a Orbital parameters listed are of HD 33632 Ab. HD 33632 Aa has ω shifted by 180° .

different formation mechanism. Future CHARIS/NIRC2 astrometry for HD 33632 Ab together with more precise HD 33632 Aa astrometry in future Gaia data releases will better constrain the companion's mass and eccentricity.

In addition to HD 33632 Aa, hundreds of nearby stars show evidence for a statistically significant acceleration plausibly caused by an unidentified substellar companion. Upcoming Gaia data releases will identify thousands more accelerating stars. Some will be young enough that extreme AO systems like SCEXAO can image self-luminous Jovian exoplanets responsible for the astrometric trends. Our work is a proof in concept that direct imaging searches targeting HGCA-selected stars may identify new substellar and potentially even planetary companions, increasing the yield of discoveries.

We thank Eric Mamajek and William Cochran for helpful comments regarding the HD 33632 system properties. The authors acknowledge the very significant cultural role and reverence that the summit of Maunakea holds within the Hawaiian community. We are most fortunate to have the opportunity to conduct observations from this mountain.


We acknowledge the critical importance of the current and recent Subaru and Keck Observatory daycrew, technicians, support astronomers, telescope operators, computer support, and office staff employees, especially during the challenging times presented by the COVID-19 pandemic. Their expertise, ingenuity, and dedication is indispensable to the continued successful operation of these observatories.









We thank the Subaru and NASA Keck Time Allocation Committees for their generous support of this program. T.C. was supported by a NASA Senior Postdoctoral Fellowship and NASA/Keck grant LK-2663-948181. T.B. gratefully acknowledges

support from the Heising-Simons foundation and from NASA under grant #80NSSC18K0439. M.T. is supported by JSPS KAKENHI grant #18H05442.

The development of SCEXAO was supported by JSPS (Grant-in-Aid for Research #23340051, #26220704, and #23103002), Astrobiology Center of NINS, Japan, the Mt Cuba Foundation, and the director's contingency fund at Subaru Telescope. CHARIS was developed under the support by the Grant-in-Aid for Scientific Research on Innovative Areas #2302. Some of the data presented herein were obtained at the W. M. Keck Observatory, which is operated as a scientific partnership among the California Institute of Technology, the University of California and the National Aeronautics and Space Administration. The Observatory was made possible by the generous financial support of the W. M. Keck Foundation.

ORCID iDs

Thayne Currie  <https://orcid.org/0000-0002-7405-3119>
 Timothy D. Brandt  <https://orcid.org/0000-0003-2630-8073>
 Masayuki Kuzuhara  <https://orcid.org/0000-0002-4677-9182>
 Olivier Guyon  <https://orcid.org/0000-0002-1097-9908>
 Christian Marois  <https://orcid.org/0000-0002-4164-4182>
 Julien Lozi  <https://orcid.org/0000-0002-3047-1845>
 Ananya Sahoo  <https://orcid.org/0000-0003-2806-1254>
 Nemanja Jovanovic  <https://orcid.org/0000-0001-5213-6207>
 Frantz Martinache  <https://orcid.org/0000-0003-1180-4138>
 Kevin Wagner  <https://orcid.org/0000-0002-4309-6343>
 Trent Dupuy  <https://orcid.org/0000-0001-9823-1445>
 G. Mirek Brandt  <https://orcid.org/0000-0003-0168-3010>
 Daniel Michalik  <https://orcid.org/0000-0002-7618-6556>

Markus Janson  <https://orcid.org/0000-0001-8345-593X>
 Gillian R. Knapp  <https://orcid.org/0000-0002-9259-1164>
 Jungmi Kwon  <https://orcid.org/0000-0003-2815-7774>
 Kellen Lawson  <https://orcid.org/0000-0002-6964-8732>
 Michael W. McElwain  <https://orcid.org/0000-0003-0241-8956>
 Taichi Uyama  <https://orcid.org/0000-0002-6879-3030>
 John Wisniewski  <https://orcid.org/0000-0001-9209-1808>
 Motohide Tamura  <https://orcid.org/0000-0002-6510-0681>

References

- Baraffe, I., Chabrier, G., Barman, T. S., Allard, F., & Hauschildt, P. H. 2003, *A&A*, 402, 701
- Barman, T. S., Konopacky, Q. M., Macintosh, B., & Marois, C. 2015, *ApJ*, 804, 61
- Bowler, B. P., Blunt, S. C., & Nielsen, E. L. 2020, *AJ*, 159, 63
- Brandt, T. D. 2018, *ApJS*, 239, 31
- Brandt, T. D., Dupuy, T. J., & Bowler, B. P. 2019, *AJ*, 158, 140
- Brandt, T. D., Dupuy, T. J., Li, Y., et al. 2020, *AJ* (submitted)
- Brandt, T. D., & Huang, C. X. 2015, *ApJ*, 807, 24
- Brandt, T. D., McElwain, M. W., Turner, E. L., et al. 2014, *ApJ*, 794, 159
- Brandt, T. D., Rizzo, M., Groff, T., et al. 2017, *JATIS*, 3, 048002
- Burrows, A., Marley, M., Hubbard, W. B., et al. 1997, *ApJ*, 491, 856
- Burrows, A., Sudarsky, D., & Hubeny, I. 2006, *ApJ*, 640, 1063
- Castro, M., Duarte, T., Pace, G., & do Nascimento, J. D. 2016, *A&A*, 590, A94
- Crepp, J. R., & Johnson, J. A. 2011, *ApJ*, 733, 126
- Crepp, J. R., Johnson, J. A., Howard, A. W., et al. 2014, *ApJ*, 781, 29
- Currie, T., Brandt, T. D., Uyama, T., et al. 2018, *AJ*, 156, 291
- Currie, T., Burrows, A., Girard, J. H., et al. 2014a, *ApJ*, 795, 133
- Currie, T., Burrows, A., Itoh, Y., et al. 2011, *ApJ*, 729, 128
- Currie, T., Cloutier, R., Brittain, S., et al. 2015, *ApJL*, 814, L27
- Currie, T., Daemgen, S., Debes, J., et al. 2014b, *ApJL*, 780, L30
- Dupuy, T. J., Brandt, T. D., Kratter, K. M., & Bowler, B. P. 2019, *ApJL*, 871, L4
- Dupuy, T. J., & Liu, M. C. 2012, *ApJS*, 201, 19
- Fernandes, R. B., Mulders, G. D., Pascucci, I., Mordasini, C., & Emsenhuber, A. 2019, *ApJ*, 874, 81
- Fischer, D. A., Marcy, G. W., & Spronck, J. F. P. 2014, *ApJS*, 210, 5
- Freund, S., Robrade, J., Schneider, P. C., & Schmitt, J. H. M. M. 2020, *A&A*, 640, A66
- Gagné, J., Lafrenière, D., Doyon, R., Malo, L., & Artigau, É. 2014, *ApJ*, 783, 121
- Gaia Collaboration, Brown, A. G. A., Vallenari, A., et al. 2018, *A&A*, 616, A1
- Golimowski, D. A., Leggett, S. K., Marley, M. S., et al. 2004, *AJ*, 127, 3516
- Greco, J. P., & Brandt, T. D. 2016, *ApJ*, 833, 134
- Groff, T. D., Chilcote, J., Kasdin, N. J., et al. 2016, *Proc. SPIE*, 9908, 990800
- Jovanovic, N., Guyon, O., Martinache, F., et al. 2015a, *ApJL*, 813, L24
- Jovanovic, N., Martinache, F., Guyon, O., et al. 2015b, *PASP*, 127, 890
- Kepler, M., Benisty, M., Müller, A., et al. 2018, *A&A*, 617, A44
- Konopacky, Q. M., Rameau, J., Duchêne, G., et al. 2016, *ApJL*, 829, L4
- Kuzuhara, N., Tamura, M., Kudo, T., et al. 2013, *ApJ*, 774, 11
- Macintosh, B., Graham, J. R., Barman, T., et al. 2015, *Sci*, 350, 64
- Mamajek, E. E., & Hillenbrand, L. A. 2008, *ApJ*, 687, 1264
- Marois, C., Doyon, R., Racine, R., & Nadeau, D. 2000, *PASP*, 112, 91
- Marois, C., Lafrenière, D., Doyon, R., Macintosh, B., & Nadeau, D. 2006, *ApJ*, 641, 556
- Marois, C., Macintosh, B., Barman, T., et al. 2008, *Sci*, 322, 1348
- Marois, C., Zuckerman, B., Konopacky, Q. M., Macintosh, B., & Barman, T. 2010, *Natur*, 468, 1080
- Nielsen, E. L., De Rosa, R. J., Macintosh, B., et al. 2019, *AJ*, 158, 13
- Nielsen, E. L., Liu, M. C., Wahhaj, Z., et al. 2012, *ApJ*, 750, 53
- Pace, G. 2013, *A&A*, 551, L8
- Pueyo, L. 2016, *ApJ*, 824, 117
- Ramírez, I., Fish, J. R., Lambert, D. L., & Allende Prieto, C. 2012, *ApJ*, 756, 46
- Scholz, R. D. 2016, *A&A*, 587, A51
- Spina, L., Meléndez, J., Karakas, A. I., et al. 2018, *MNRAS*, 474, 2580
- Stephens, D. C., Leggett, S. K., Cushing, M. C., et al. 2009, *ApJ*, 702, 154
- Takeda, G., Ford, E. B., Sills, A., et al. 2007, *ApJS*, 168, 297
- Thalmann, C., Carson, J., Janson, M., et al. 2009, *ApJL*, 707, L123
- Zurlo, A., Vigan, A., Galicher, R., et al. 2016, *A&A*, 587, A57